Highly efficient 1.54 μm emission in Zr/Yb/Er-codoped $LiNbO_3$ crystal

Yannan Qian,[1] Rui Wang,[2] Biao Wang,[1,*] Chao Xu,[2] Lili Xing,[2] and Yanling Xu[2]

[1] *School of Physics and Engineering, Sun Yat-sen University, Guangzhou 510275, China*
[2] *Department of Chemistry, Harbin Institute of Technology, Harbin 150001, China*
**Corresponding author: wangbiao@mail.sysu.edu.cn*

Received August 21, 2012; accepted August 26, 2012;
posted August 30, 2012 (Doc. ID 174475); published October 2, 2012

Codoping with Zr^{4+} ions enhances the 1.54 μm emission in Yb/Er:$LiNbO_3$ crystal by about three times. Optical damage resistant Zr^{4+} ion increases the maximum phonon energy of Er:$LiNbO_3$ host, which is favorable for the nonradiative relaxation from $^4I_{11/2}$ to $^4I_{13/2}$ state (Er). The time decay spectra show that the incorporation of Zr^{4+} ions leads to a shortening lifetime of $^4I_{11/2}$ state (Er), increasing the nonradiative relaxation rate of $^4I_{11/2} \rightarrow {}^4I_{13/2}$ (Er) in Yb/Er:$LiNbO_3$. The 1.54 μm emission enhancement is important to telecommunication application. © 2012 Optical Society of America

OCIS codes: 260.2510, 160.3730.

Erbium-doped $LiNbO_3$ (Er:$LiNbO_3$) crystals have become important building blocks for Er-doped waveguide amplifiers, which are one of the key components for local and wide area networks, cable television distribution, and anticipated fiber-to-the-home applications [1]. Er:$LiNbO_3$ crystal emits the eye-safe 1.54 μm emission, matching well with the "windows of transparency" [2]. The combination of the amplifying around 1.54 μm presented by Er^{3+} ions with the excellent nonlinear property of $LiNbO_3$ allows the development of interesting waveguide devices with higher functionality [3].

However, the practical applications of Er:$LiNbO_3$ crystal suffer from the photorefractive effect. Although the breakthroughs have been achieved by doping with anti-photorefractive ions, such as Mg^{2+} (4.6 mol. %), Zn^{2+} (6.5 mol. %), In^{3+} (3 mol. %), and Hf^{4+} (4 mol. %) [4–7], their high threshold concentrations are deleterious to grow crystal of good optical quality. Therefore, tetravalent zirconium (Zr) has been the most promising candidate to suppress the photorefractive effect since it not only has a much higher optical damage resistance than Mg:$LiNbO_3$ and Hf:$LiNbO_3$, but also has a lower doping threshold (2.0 mol. %) and a distribution coefficient close to one [8]. Recently, it has been reported that the upconversion emission in Tm:$LiNbO_3$ crystal codoped with Zr^{4+} ions is about three times higher than that in Zn/Tm:$LiNbO_3$ crystal [9]. This is because the small discrepancy of the atomic radius between Zr (1.57 Å) and Li (1.54 Å), compared with that between Zn (1.33 Å) and Li, decreases the structural disorder of $LiNbO_3$ lattice. However, there are few reports on the effect of Zr^{4+} ion on the near infrared emission in Er:$LiNbO_3$ crystal. In this Letter, we primarily found that Zr^{4+} ions enhance the 1.54 μm emission via increasing nonradiative relaxation rate of $^4I_{11/2} \rightarrow {}^4I_{13/2}$ transition of Er^{3+} ion in Er:$LiNbO_3$ and Yb/Er:$LiNbO_3$ crystals.

Er(1 mol. %):$LiNbO_3$ and Er(1 mol. %)/Yb(1 mol. %):$LiNbO_3$ crystals codoped with and without 4 mol. % ZrO_2 were grown along ferroelectric *c* axis by Czochralski technique. The grown four crystals are named as Er-1, Zr/Er-4/1, Yb/Er-1/1, and Zr/Yb/Er-4/1/1, respectively. The raw materials (Er_2O_3, Yb_2O_3, ZrO_2, Li_2CO_3, and Nb_2O_5) were mixed for 24 h. Mixtures were heated at 750 °C for 2 h to remove CO_2, and then further heated up to 1150 °C for 2 h to form polycrystalline powder. The optimum growth conditions were depicted as follows: an axial temperature gradient of $40 \sim 50$ K/cm, the rotating rate of $10 \sim 25$ rpm, and the pulling rate of $0.5 \sim 2$ mm/h. The grown crystals were polarized at 1200 °C with a current density of 5 mA/cm^2. The boules were cut into Y-cut plates ($X \times Y \times Z = 10 \times 2 \times 10$ mm^3) with polished surfaces.

The Er^{3+}, Yb^{3+}, and Zr^{4+} contents in the crystal were determined by use of the inductively coupled plasma mass spectrometry (ICP-MS; Optima 7500 Series, Agilent Technologies Inc., Beijing), and the results were shown in Table 1. A power-controllable 980 nm diode laser was used as the excitation source. The fluorescence spectra were recorded by the spectrometer (Bruker optics 500IS/SM) equipped with a semiconductor cooled charge coupled device detector (DV440, Andor). Decay profiles at 1020 nm were measured by square-wave-modulation of the electric current input to the 980 nm diode laser and recorded via a Tektronix TDS 5052 digital scilloscope with a lock-in preamplifier (Stanford Research System Model SR830 DSP). Raman spectra were measured by the Renishaw-1000 spectrometer (Renishaw Inc., England). The absorption spectrum in the range from 300 to 1650 nm was measured with PerkinElmer Lambda 900 spectrophotometer.

The near infrared emissions at 1.54 μm arising from the $^4I_{13/2} \rightarrow {}^4I_{15/2}$ transition of Er^{3+} ion [10] in Yb/Er-1/1 and Zr/Yb/Er-4/1/1 crystals are shown in Fig. 1. The inset displays the 1.54 μm emission spectra of Er-1 and Zr/Er-4/1 crystals. As illustrated in Fig. 1, the intensity of 1.54 μm emission in Zr/Yb/Er-4/1/1 is more than three times higher than that in Yb/Er-1/1 crystal. It can be seen from the inset that the Zr^{4+} ions also improve 1.54 μm emission in Er:$LiNbO_3$ crystal. These enhancements will provide many more probabilities for practical applications.

In order to characterize the maximum phonon energy of host material, Raman spectra of Zr/Er-4/1 and Er-1 are measured and shown in Fig. 2. All observed modes in the spectra have been assigned in the previous literature [11]. It is clear that as Zr^{4+} ions are incorporated into Er:$LiNbO_3$ crystal, the highest peak shifts from 631 to

Table 1. Content of Er^{3+}, Yb^{3+}, and Zr^{4+} Ion in Melt/Crystal

	Er-1	Zr/Er-4/1	Yb/Er-1/1	Zr/Yb/Er-4/1/1
Zr^{4+} in melt (mol. %)	0	4	0	4
Yb^{3+} in melt (mol. %)	0	0	1	1
Er^{3+} in melt (mol. %)	1	1	1	1
Zr^{4+} in crystal (mol. %)	0	3.644	0	3.612
Yb^{3+} in crystal (mol. %)	0	0	1.49	1.33
Er^{3+} in crystal (mol. %)	1.51	1.46	1.50	1.37

872 cm^{-1}. The peak at 872 cm^{-1} corresponds to the stretching vibration of Nb-O (LO mode) in isolated groups. Generally, Er^{3+} ions at the $^4I_{13/2}$ state, which radiatively relax to $^4I_{15/2}$ state producing 1.54 μm emission, is populated by relaxing nonradiatively from the metastable $^4I_{11/2}$ state under 980 nm excitation [12]. Owing to the long fluorescence lifetime of $^4I_{11/2}$ state, the excited state absorption (ESA) from $^4I_{11/2}$ to $^4F_{7/2}$ state reduces the population of $^4I_{13/2}$ state [13]. The higher maximum phonon energy (872 cm^{-1}) in Zr/Er:LiNbO$_3$ crystal could lead to a fast $^4I_{11/2} \rightarrow {}^4I_{13/2}$ transition of Er^{3+} ion and a reduced ESA rate. Therefore, the behavior that Zr^{4+} ions enhance the 1.54 μm emission in Er:LiNbO$_3$ may be attributed to the increased maximum phonon energy of crystal lattice.

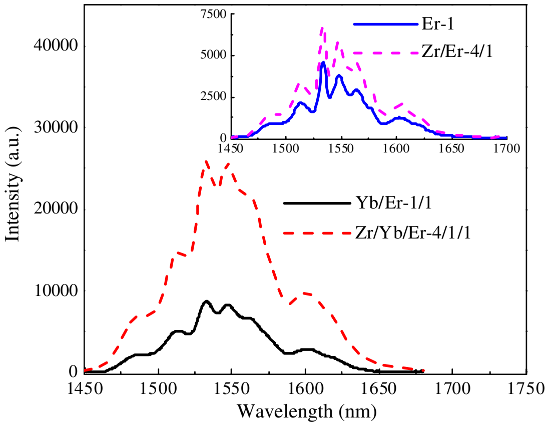

Fig. 1. (Color online) Near infrared emission spectra of Zr/Yb/Er-4/1/1 and Yb/Er-1/1 under 980 nm excitation. The inset is the 1.54 μm emission spectra of Zr/Er-4/1 and Er-1 crystals.

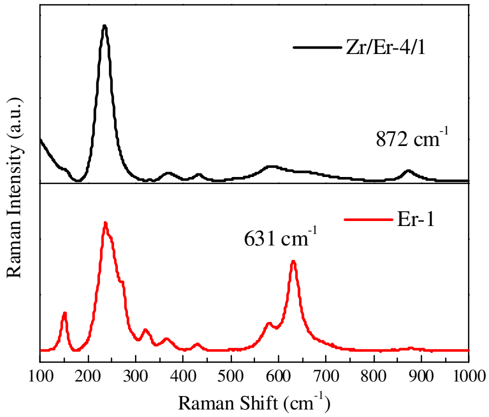

Fig. 2. (Color online) Raman spectra of Zr/Er-4/1 and Er-1 crystals at room temperature.

As for Yb/Er:LiNbO$_3$ crystal, the energy levels of Er^{3+} and Yb^{3+} ions, as well the upconversion mechanism under 980 nm excitation are depicted in Fig. 3, which illustrate that the intermediate $^4I_{11/2}$ state of Er^{3+} ion is mainly populated via energy transferring from $^2F_{5/2}$ state of Yb^{3+} ion (ET1:$^4I_{15/2}$Er + $^2F_{5/2}$Yb $\rightarrow$ $^4I_{11/2}$Er+ $^2F_{7/2}$Yb). This is because Yb^{3+} ion has a large absorption cross section around 980 nm and can efficiently transfer its energy to the $^4I_{11/2}$ state of Er^{3+} ion [14]. It is obvious that ET2 process ($^4I_{11/2}$Er + $^2F_{5/2}$Yb $\rightarrow$ $^4F_{7/2}$Er+ $^2F_{7/2}$Yb) competes with the nonradiative relaxation of $^4I_{11/2} \rightarrow {}^4I_{13/2}$ transition of Er^{3+} ion.

Figure 4 displays the decay profiles of $^4I_{11/2} \rightarrow {}^4I_{15/2}$ transition of Er^{3+} ion at 1020 nm in Yb/Er:LiNbO$_3$ doped with and without Zr^{4+} ions. The inset presents the contrasted near infrared spectra of Er-1 and Zr/Yb/Er-4/1/1 crystals under 980 nm excitation. As shown in the inset, the almost same decay profiles of the $^4I_{11/2}$ (Er) and $^2F_{5/2}$ (Yb) states at 1020 and 1075 nm may arise from their strong coupling. Comparison of near infrared emission spectra in Er-1 with that in Zr/Yb/Er-4/1/1 indicates that the 1020 and 1075 nm emission peaks correspond to $^4I_{11/2} \rightarrow {}^4I_{15/2}$ of Er^{3+} ion and $^2F_{5/2} \rightarrow {}^2F_{7/2}$ transition of Yb^{3+} ion, respectively. It can be seen from Fig. 4 that the lifetimes of $^4I_{11/2}$ state (Er) in Yb/Er-1/1 and Zr/Yb/Er-4/1/1 are measured to be 335 and 300 μs, respectively. It is assuming that the effect of Yb^{3+} on the lifetime of $^4I_{11/2}$ state (Er) in Yb/Er-1/1 and Zr/Yb/Er-4/1/1 is similar. Therefore, the Zr^{4+} codoping is responsible to the shortening lifetime of $^4I_{11/2}$ state (Er).

The nonradiative relaxation rate can be calculated by the following equation [15]:

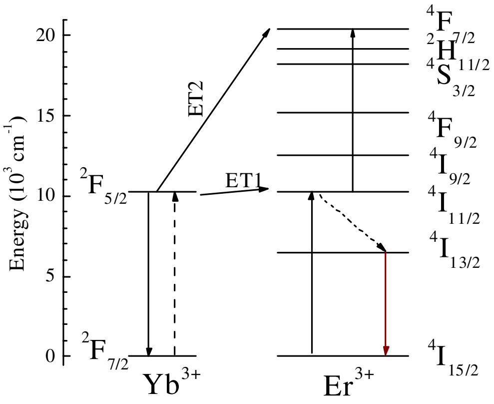

Fig. 3. (Color online) Energy levels of Er^{3+} and Yb^{3+} ions, as well as upconversion mechanism under 980 nm excitation.

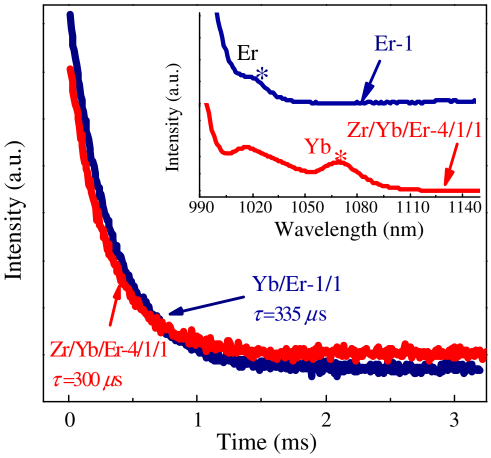

Fig. 4. (Color online) Decay profiles of $^4I_{11/2} \rightarrow {}^4I_{15/2}$ transition of Er^{3+} ion at 1020 nm in Zr/Yb/Er-4/1/1 and Yb/Er-1/1 crystals. The inset is near infrared emission spectra of Zr/Yb/Er-4/1/1 and Er-1 in the range from 900 to 1100 nm.

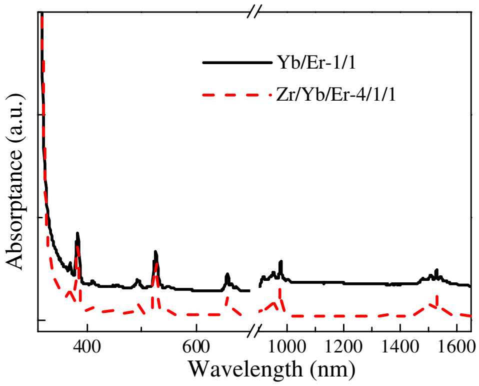

Fig. 5. (Color online) UV-vis-near infrared absorption spectra of Yb/Er-1/1 and Zr/Yb/Er-4/1/1 crystals.

$$W_N = \frac{1}{\tau_{\text{meas}}} - \frac{1}{\tau_{\text{rad}}}, \tag{1}$$

where W_N is the nonradiative relaxation rate, τ_{meas} is the measured lifetime, and τ_{rad} is the radiative lifetime calculated by Judd–Ofelt (J–O) theory. The UV-visible-near infrared absorption spectra of Zr/Yb/Er-4/1/1 and Yb/Er-1/1 crystals, which are used to calculate the τ_{rad}, are shown in Fig. 5. The details on J–O theory and calculation procedures have been reported in [16]. Consequently, the radiative lifetimes (τ_{rad}) of $^4I_{11/2}$ (Er) in Zr/Yb/Er-4/1/1 and Yb/Er-1/1 are equal to 2424.5 and 2750.4 μs, respectively. According to Eq. (1), W_N are 2921 and 2621 s^{-1}, respectively, for Zr/Yb/Er-4/1/1 and Yb/Er-1/1 crystals. The increased W_N value corresponds to a fast nonradiative relaxation from $^4I_{11/2}$ to $^4I_{13/2}$ state (Er) and, in turn, a low ET2 process in Zr/Yb/Er-4/1/1 crystal. The overall result is the increased population of $^4I_{13/2}$ state (Er) and the improved 1.54 μm emission in Zr/Yb/Er-4/1/1 crystal, in agreement with the experimental results shown in Fig. 1.

In summary, an enhanced 1.54 μm emission is observed in Zr/Yb/Er:$LiNbO_3$ crystal under 980 nm excitation. The experimental results indicate that Zr^{4+} codoping increase the maximum phonon energy of Er:$LiNbO_3$ host. The measured lifetime of $^4I_{11/2}$ state (Er) shortens from 335 μs in Yb/Er:$LiNbO_3$ to 300 μs in Zr/Yb/Er:$LiNbO_3$ crystal. In combination with the J–O calculated radiative lifetime, the nonradiative relaxation rate of $^4I_{11/2} \rightarrow {}^4I_{13/2}$ transition (Er) increases from 2621 to 2921 s^{-1}, which is responsible to gain highly efficient 1.54 μm emission in Zr/Yb/Er:$LiNbO_3$ crystal.

This work is financially supported by National Natural Science Foundation of China (10732100, 11232015, 11072271, and 10972239) and Natural Science Foundation of Heilongjiang Province of China (B200903).

References

1. D. L. Zhang, P. Zhang, W. H. Wong, and E. Y. B. Pun, Cryst. Growth Des. **8**, 2121 (2008).
2. Y. C. Yan, A. J. Faber, H. de Waal, P. G. Kik, and A. Polman, Appl. Phys. Lett. **71**, 2922 (1997).
3. I. Baumann, R. Brinkmann, M. Dinand, W. Sohler, L. Beckers, Ch. Buchal, M. Fleuster, H. Holzbrecher, H. Paulus, K.-H. Müller, Th. Gog, G. Materlik, O. Witte, H. Stolz, and W. von der Osten, Appl. Phys. A **64**, 33 (1996).
4. J. C. Deng, W. L. Zhang, J. K. Wen, G. Y. Zhang, and H. F. Wang, Opt. Lett. **19**, 933 (1994).
5. T. R. Volk, V. I. Pryalkin, and N. M. Rubinina, Opt. Lett. **15**, 996 (1990).
6. Y. F. Kong, J. K. Wen, and H. F. Wang, Appl. Phys. Lett. **66**, 280 (1995).
7. W. B. Yan, L. H. Shi, H. J. Chen, X. Z. Zhang, and Y. F. Kong, Opt. Lett. **35**, 601 (2010).
8. Y. F. Kong, S. G. Liu, Y. J. Zhao, H. D. Liu, S. L. Chen, and J. J. Xu, Appl. Phys. Lett. **91**, 081908 (2007).
9. J. W. Shur, K. H. Choi, and D. H. Yoon, J. Cryst. Growth **318**, 653 (2011).
10. K. Kuriki, S. Nishihara, Y. Nishizawa, T. Yoshinaga, A. Tagaya, Y. Koike, and Y. Okamoto, Opt. Lett. **28**, 570 (2003).
11. P. Capek, G. Stone, V. Dierolf, C. Althouse, and V. Gopolan, Phys. Stat. Sol. C **4**, 830 (2007).
12. A. Giaquinto, L. Mescia, G. Fornarelli, and F. Prudenzano, Opt. Lett. **36**, 142 (2011).
13. G. Y. Chen, L. M. Yang, C. Xu, S. W. Hao, H. L. Qiu, L. Sun, Y. H. Xu, and C. H. Yang, Opt. Lett. **37**, 1268 (2012).
14. N. A. Tolstik, S. V. Kurilchik, V. E. Kisel, N. V. Kuleshov, V. V. Maltsev, O. V. Pilipenko, E. V. Koporulina, and N. I. Leonyuk, Opt. Lett. **32**, 3233 (2007).
15. V. K. Rai and S. B. Rai, Solid State Commun. **132**, 647 (2004).
16. A. Li, L. Sun, Z. Zheng, Q. Lü, W. Wu, W. Liu, Y. Yang, and T. Lü, Appl. Phys. B **90**, 29 (2008).